OncoTargets and Therapy

Dovepress
open access to scientific and medical research

Open Access Full Text Article

ORIGINAL RESEARCH

Radiosynthesis and pharmacokinetics of [^{18}F]fluoroethyl bufalin in hepatocellular carcinoma-bearing mice

This article was published in the following Dove Press journal:
OncoTargets and Therapy
11 January 2017
Number of times this article has been viewed

Zhaoshuo Yang[1]
Jianhua Liu[2]
Qingqing Huang[3]
Zhouji Zhang[1]
Jiawei Zhang[1]
Yanjia Pan[1]
Yunke Yang[1]
Dengfeng Cheng[4]

[1]Department of Chinese Traditional Medicine, Zhongshan Hospital, Fudan University, [2]School of Medicine, Shanghai Jiao Tong University, [3]Department of Nuclear Medicine, Shanghai 10th People's Hospital, Tongji University School of Medicine, [4]Department of Nuclear Medicine, Zhongshan Hospital, Fudan University, Shanghai, People's Republic of China

Purpose: Bufalin, the main component of a Chinese traditional medicine chansu, shows convincing anticancer effects in a lot of tumor cell lines. However, its in vivo behavior is still unclear. This research aimed to evaluate how bufalin was dynamically absorbed after intravenous injection in animal models. We developed a radiosynthesis method of [^{18}F]fluoroethyl bufalin to noninvasively evaluate the tissue biodistribution and pharmacokinetics in hepatocellular carcinoma-bearing mice.

Methods: [^{18}F]fluoroethyl bufalin was synthesized with conjugation of ^{18}F-CH_2CH_2OTs and bufalin. The radiochemical purity was proved by the radio-high-performance liquid chromatography (HPLC). The pharmacokinetic studies of [^{18}F]fluoroethyl bufalin were then performed in Institute of Cancer Research (ICR) mice. Furthermore, the biodistribution and metabolism of [^{18}F]fluoroethyl bufalin in HepG2 and SMMC-7721 tumor-bearing nude mice were studied in vivo by micro-positron emission tomography (micro-PET).

Results: The radiochemical purity (RCP) of [^{18}F]fluoroethyl bufalin confirmed by radio-HPLC was 99%±0.18%, and [^{18}F]fluoroethyl bufalin showed good in vitro and in vivo stabilities. Blood dynamics of [^{18}F]fluoroethyl bufalin conformed to the two compartments in the ICR mice model. The pharmacokinetic parameters of [^{18}F]fluoroethyl bufalin were calculated by DAS 2.0 software. The area under concentration–time curve (AUC_{0-t}) and the values of clearance (CL) were 540.137 μg/L·min and 0.001 L/min/kg, respectively. The half-life of distribution ($t_{1/2\alpha}$) and half-life of elimination ($t_{1/2\beta}$) were 0.693 and 510.223 min, respectively. Micro-PET imaging showed that [^{18}F]fluoroethyl bufalin was quickly distributed via the blood circulation; the major tissue biodistribution of [^{18}F]fluoroethyl bufalin in HepG2 and SMMC-7721 tumor-bearing mice was liver and bladder.

Conclusion: [^{18}F]fluoroethyl bufalin was accumulated rapidly in the liver at an early time point (5 min) post injection (pi) and then declined slowly, mainly through both the hepatic pathway and the renal pathway. Our study showed the biodistribution of [^{18}F]fluoroethyl bufalin in micro-PET images and provided visible information for demonstrating the bioactivities of bufalin.

Keywords: [^{18}F]fluoroethyl bufalin, PET, hepatocellular carcinoma, pharmacokinetic, tissue biodistribution

Correspondence: Yunke Yang
Department of Chinese Traditional Medicine, Zhongshan Hospital, Fudan University,180 Fenglin Road, Shanghai 200032, People's Republic of China
Email yang.yunke@zs-hospital.sh.cn

Dengfeng Cheng
Department of Nuclear Medicine, Zhongshan Hospital, Fudan University, 180 Fenglin Road, Shanghai 200032, People's Republic of China
Tel +86 21 6404 1990
Fax +86 21 6403 8472
Email cheng.dengfeng@zs-hospital.sh.cn

Introduction

Bufalin, which is extracted from the body covering of the Bufo bufo gargarizans Cantor, is a main active component of a traditional Chinese medicine (Chansu).[1] Bufalin has multi-target antitumor effect in a range of tumors, such as hepatocellular carcinomas,[2] colorectal cancer,[3] leukemia,[4] gastric cancer,[5] and osteosarcoma.[6] Preceding findings have revealed that the anticancer activity of bufalin could be attributed to its prevention

of cell proliferation, instruction of apoptosis, disturbance of the cell cycle, and modulation of the immune response.[7–9] Earlier study of ours revealed that bufalin had convincing anticancer growth and reduced the metastatic potentials in the human hepatocellular carcinoma-transplanted tumor model, and the fundamental mechanism was in part mediated by the signaling pathway of the Akt–GSK3β–β-catenin–E-cadherin.[10,11] These results indicated that bufalin might be a purposeful constituent for cancer treatment. However, there was not much known about the distribution of bufalin in vivo, especially in a variety of tumors. Moreover, detection of bufalin and its metabolites was difficult in vivo.

Positron emission tomography (PET) is a noninvasive imaging method, which has been applied for clinical practice in many areas.[12] As a useful tool for imaging and calculating cell and molecular procedures in the body, PET has vast probability to enlarge our knowledge of the pathophysiology of tumors' diagnosis and assist the progress of anticancer drugs.[13] A number of antitumor drugs have been labeled with radionuclides successfully as imaging tracers for PET explorations, such as hormones, antibodies, kinase inhibitors, and other anticancer substances.[14–16] It is not surprising that the role of such technology in hastening anticancer drug events is approved in a crucial trial initiative by the US Food and Drug Administration (FDA).[17] The initial concept of microdosing of a drug has been presented applying radiolabeled drugs in conjunction with PET to attain preliminary data about distribution, pharmacokinetics, and tumor targets at an earliest stage of drug development.[18] PET is currently one of the most helpful noninvasive in vivo imaging techniques for the investigation of drug pharmacokinetics.

The purpose of this research was to evaluate the distributions, pharmacokinetics, and tumor-targeting performance of the potential anticancer drug bufalin in nude mice bearing with hepatocellular carcinomas. The evidences from the present imaging study could promote prospective investigation and be applied to monitor bufalin therapy efficacy in mice and future clinical practices.

Methods

General information

The reagents in the experiment were of analytical grade without additional refinement, unless specified otherwise. Bufalin (purity >98%) was obtained from Baoji Herbest Bio-Tech Co., Ltd (Baoji, People's Republic of China).[18]F-fluoride was received from a cyclotron (HM20; Sumitomo Heavy Industries, Ltd, Tokyo, Japan) situated in the Jiangsu Institute of Nuclear Medicine by proton irradiation of ^{18}O-enriched water. A high-performance liquid chromatography (HPLC) system (Waters, Milford, MA, USA) supplied with a Waters 2998 photodiode array (PDA) detector and a tetramethylammonium solid-phase extraction column (250×10 mm, 5 μm; Waters) was needed for [^{18}F]fluoroethyl refinement. The rate of flow was 3 mL/min, and the mobile phase started from 95% dissolvent A (0.1% trifluoroacetic acid in water) and 5% dissolvent B (0.1% trifluoroacetic acid in methanol; 0–2 min), and it was progressively shifted to 30% dissolvent A and 70% dissolvent B at 35 min. The ultraviolet absorbance was observed at 280 nm, and the ultraviolet spectrum was tested with the PDA detector.

Analytical HPLC was carried out in Waters Breeze System with a YMC-Pack Pro-C18 RS column (5 μm, 10×250 mm; Waters); the compound was controlled by using a Cd (Te) detector. The flow rate was 1 mL/min. The isocratic mobile phase was 0.05 mol/L phosphate-buffered saline (PBS; pH =7.0).

A micro-PET equipment (Inveon; Siemens Co., Knoxville, TN, USA) and a fluorescence microscope (X51; Olympus Corporation, Tokyo, Japan) were applied. The animal tests in this research were carried out by the Shanghai Medical Experimental Animal Care Committee.

Animals

Male BALB/c nude mice (20–22 g, 4 weeks old) were obtained from the SLAC Laboratory Animal Company (Shanghai, People's Republic of China). Normal Institute of Cancer Research (ICR) mice (weighing 20–24 g) were provided by SLAC Laboratory Animal Company. All mice were handled according to the Use of Laboratory Animals and the National Institutes of Health Guidelines for Care. The investigational protocol was approved by the Shanghai Medical Experimental Animal Care Committee.

Cell culture

The SMMC-7721 and HepG2 human hepatoma cell lines were purchased from the Type Culture Collection of the Chinese Academy of Sciences (Shanghai, People's Republic of China). Both cell lines were cultured in Dulbecco's Modified Eagle's Medium (DMEM) added with 10% fetal bovine serum (FBS) in a moisten atmosphere of 95% air and 5% CO_2 at 37°C. The two cell lines were used to establish the models.

Establishment of metastatic orthotopic tumor model

Two types of metastatic mice model of human hepatoma cells, SMMC-7721 and HepG2, were employed for this study. Briefly, SMMC-7721 and HepG2 cells (5×10^6)

were injected subcutaneously into the left abdomen area of nude mice. When the subcutaneous tumors proliferated to almost 3 cm in width (~5 weeks after injection), they were removed and cut into small pieces of equal volume (1.5–2×2×2 mm^3) and then these slices were placed into the sterile saline solution.

For the following liver orthotopic transplantation of above tumor slices, all the surgical procedures were performed under general anesthesia using intraperitoneal injection of 3% pelltobarbitalum natricum (45 mg/kg; Sigma-Aldrich Co., St Louis, MO, USA). Once anesthetized, the male BALB/c nude mice were fixed on an experimental board in a supine position. An 8-mm transverse incision was made below the left last rib margin, following sterilization of the area with 0.5% iodophor, which was perpendicular to the median line and was 1–1.5 cm long. The right liver lobes were carefully pulled out of the abdominal cavity with a sterile cotton swab. The smaller pieces of tumor (1.5–2×2×2 mm^3) were put into the right liver lobes at a depth of 3.5 mm using the surgery forceps. The tumor tissues were fixed in the right liver lobes with a plus 6-0 suture line. A small piece of sterile gauze was placed on the injection site, and light pressure was applied for 1 min to prevent bleeding and spilling. The skin was then sterilized with 70.5% iodophor, and the wound was sutured with a plus 5-0 suture line.

Synthesis of fluoroethyl bufalin and radiosynthesis of [18F]fluoroethyl bufalin

Fluoroethyl bufalin and [18F]fluoroethyl bufalin were synthesized in house. First, [18F]fluoroethyl bufalin was synthesized according to the reference for fluoroethyl bufalin. The details are as follows (Scheme 1). A Schlenk tube (10 mL) equipped with a magnetic stir bar was charged with NaH (50.0 mg, 1.3 mmol, 60% in mineral oil) and dry *N*,*N*-dimethylformamide (DMF; 1 mL) under N_2. The mixture was cooled to 0°C and then bufalin (50.0 mg, 0.13 mmol) was added. After the mixture was stirred for 15 min, 2-bromofluoroethane (45 µL, 0.61 mmol) was added via syringe. After the reaction proceeded for 24 h at 20°C, the resulting solution was poured into ice water (10 mL) and then extracted by CH_2Cl_2 (3×10 mL). The combined organic phase was dried over Na_2SO_4 and concentrated under vacuo. The resulting residue was purified by silica gel flash column chromatography using petroleum ether:ethyl acetate (1/1) as eluent. The product fluoroethyl bufalin was obtained as a colorless solid (28.3 mg, 50%) – ^{1}H NMR (400 MHz, $CDCl_3$) δ6.70 (s, 1H), 4.31 (dt, J_d =28 Hz, J_t =4 Hz, 2H), 6.19 (d, J =12 Hz, 1H), 5.38 (d, J=12 Hz, 1H), 4.61 (dt, J_d=48 Hz, J_t=4 Hz, 2H), 4.13 (s, 1H), 2.87 (s, 1H), 2.13-1.44 (m, 22H), 0.98 (m, 6H); ^{13}C NMR (100 MHz, $CDCl_3$) δ166.4, 152.9, 143.7, 121.5, 109.0, 91.9, 82.5, 80.8, 66.9, 62.8, 62.6, 46.2, 40.4, 37.6, 36.2, 35.4,

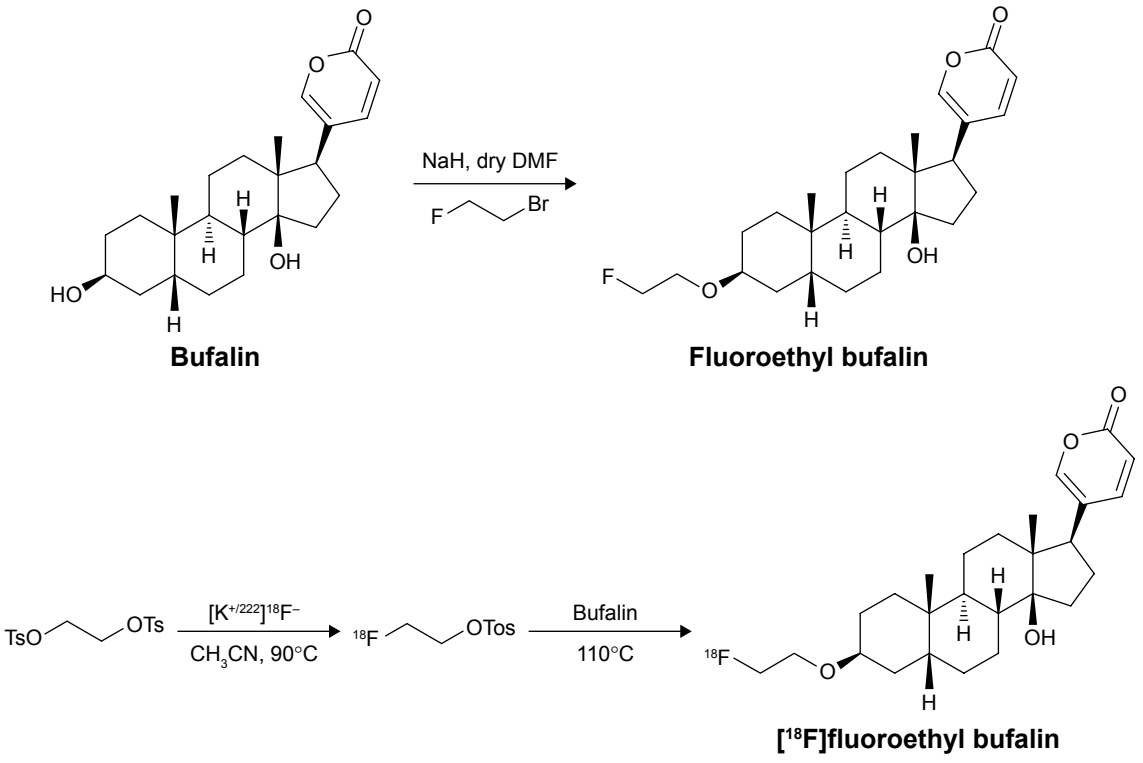

Scheme 1 A scheme of fluoroethyl bufalin and [18F]fluoroethyl bufalin synthesis.
Abbreviation: DMF, *N*,*N*-dimethylformamide.

33.4, 32.9, 32.0, 31.8, 29.8, 29.7, 17.9, 26.2, 23.8, 20.7, 20.4, 15.5; HPLC purity 95%; MS (ESI) *m/z* 433 $(M+H)^+$.

The second part of Scheme 1 shows the reaction scheme of [^{18}F]fluoroethyl bufalin. Briefly, $^{18}F^-$ was produced from the ^{18}O (p,n) ^{18}F reaction using a HM-20 cyclotron (Sumitomo Heavy Industries) in 95% enriched [^{18}O]H_2O. The $^{18}F^-$ was absorbed to tetramethylammonium solid phase extraction column. Then, the aqueous $^{18}F^-$ solution (1.87–3.48 GBq) composed of the K_2CO_3 (10–12 mg) and Kryptofix 222 (1–2 mg) was put in a brown container. The reaction mixture was dried by helium gas flow and heated at 105°C for 10 min. Afterward, the reaction mixture was put into anhydrous acetonitrile (2 mL) and heated to 105°C under helium gas flow to remove water. The remainder was added into a solution of 1,2-bis(tosyloxy)ethane (10 mg) in anhydrous acetonitrile (1 mL). The reaction vial was sealed and heated at 90°C for 10 min. Then the reaction mixture was cooled down and anhydrous ether (8 mL) was added. The intermediate ^{18}F-CH_2CH_2OTs could be obtained after the mixture was dried with nitrogen flow.

^{18}F-CH_2CH_2OTs achieved above was redissolved in acetonitrile (1 mL) and was added into a solution of bufalin (20 mg, 0.3 μmol) in DMF (0.5 mL). The reaction was conducted at 110°C for 20 min until most of the ^{18}F-CH_2CH_2OTs had reacted with bufalin (detected by radio-thin layer chromatography [TLC], acetonitrile 95%). The final purification was completed through C18 reversed-phase chromatography (the testing method was installed for radioactivity, and the ultraviolet spectrophotometer absorbance was set at a wavelength of 280 nm). HPLC segments encompassing radioactivity were associated and dried up with a stream of argon to eliminate the acetonitrile. The in vitro stabilities of freshly prepared [^{18}F]fluoroethyl bufalin were achieved respectively in PBS (0.1 mol/L, pH =7.2) and mouse serum at different periods (0–8 h) in a water bath at 37°C.

Biodistribution studies

The biodistribution of [^{18}F]fluoroethyl bufalin was studied in BALB/c nu/nu mice (20–22 g, 4 weeks old). Fifteen mice were used for intravenous injection. For intravenous administration, [^{18}F]fluoroethyl bufalin was injected into the tail vein of the mice under isoflurane anesthesia. The injection dose (7.4 MBq; radiochemical purity [RCP] 99%) was 0.2 mL.

The mice were killed at 45, 120, and 240 min after administration of [^{18}F]fluoroethyl bufalin (five mice at each time point). The mice were killed at the desired time points after injection. The organs of heart, liver, spleen, lung, kidneys, stomach, intestine, femur, muscle (leg muscles), and tumor were harvested, counted, and weighed for radioactivity values. The radioactivity in the tissues was measured with the γ-counter. The percentage of injected dose per organ (%ID/organ) and the percentage of injected dose per gram of tissue per body weight (%ID/g) were calculated by contrast with a counted, weighed standard.

Pharmacokinetic studies

For pharmacokinetics studies, [^{18}F]fluoroethyl bufalin (7.4 MBq, 0.2 mL) was injected into the six ICR mice by intravenous injection through the caudal vein. An array of blood samples (10 μL) was accumulated in blood collection tubes by pinching the tail with a syringe at 3, 5, 10, 20, 30, 40, 60, 120, 240, 360, 480, and 600 min post injection (pi). The radioactivity of blood samples was evaluated and calculated as %ID/g. The radioactivity was displayed as a function of time. Meanwhile, pharmacokinetics parameters were counted through the pharmacokinetic calculation program (Drug And Statistics, version 2.1.1; Mathematical Pharmacology Professional Committee of China, Beijing, People's Republic of China). Pharmacokinetic equation was utilized to match the curve:

$$C = Ae^{-\alpha t} + Be^{-\beta t},$$

where C is the blood value of the [^{18}F]fluoroethyl bufalin at any particular point of time t, A and B are invariables, α is half-life of distribution phase, and β is half-life of elimination phase. The area under concentration–time curve (AUC_{0-t}) and the values of clearance (CL) were also calculated.

Dynamical micro-PET images of SMMC-7721 and HepG2 tumor-bearing nude mice

Small-animal PET scans for the [^{18}F]fluoroethyl bufalin were performed in both SMMC-7721 and HepG2 tumor model (three mice per group). The animals were anesthetized under 1.5% isoflurane. Then the mice were placed prostrate and fixed. After that the mice were injected with 7.4 MBq [^{18}F]fluoroethyl bufalin (0.2 mL) through the tail vein and immediately scanned dynamically for 360 min. The scans were rebuilt by a two-dimensional ordered-subset expectation maximization (2D OSEM) process without rectification for decay or dispersing. For the images, regions of interest (ROIs) were drafted over the major tissues and tumor by the vendor-supplied software (ASI Pro 5.2.4.0 Siemens Healthineers, Erlangen, Germany) on attenuated corrected entire body coronal images. The radioactivity attention in the

major organs and tissues was got from average pixel values within the ROI level. After that, the data were translated to megabecquerel per milliliter per minute by the standardization factors measured in the Inveon PET equipment. The data were split by the radioactivity to get (presuming an organizational density of 1 g/mL) a %ID/g ROI image.

Statistical analysis

The information was showed in the forms of mean ± SD and evaluated by SPSS v.22.0 software.

Results

Radiosynthesis of [18F]fluoroethyl bufalin

The conjugation of bufalin to ^{18}F-CH_2CH_2OTs occurred in this chemical, which is presented in Figure 1A. The product was purified by a reversed phase HPLC system. The chemical and radiochemical purities of [18F]fluoroethyl bufalin were 99%±0.18% (the consistent retention time =17.86 min, three times repetition). The purity and character of [18F]fluoroethyl bufalin were confirmed by HPLC. Starting from bufalin (Figure 1B), the radio-labeled drug was able to be synthesized within 180 min, including HPLC purification time. The consistent retention time of [18F]fluoroethyl bufalin synthesized in the same HPLC confirmed that the structures of the drugs were identical.

In vitro stability

[18F]fluoroethyl bufalin did not decompose when the drug was synthesized or formulated. The chromatographic analyses presented that the compound produced under optimum conditions was of good stability, keeping an RCP of 99% until 10 h in PBS at room temperature (26°C±3°C). The results of the stability of [18F]fluoroethyl bufalin in PBS at room temperature are presented in Figure 2A. For further investigation of the stability of [18F]fluoroethyl bufalin in serum, [18F]fluoroethyl bufalin was cultured in mouse serum at 36°C±2°C for 6 h and evaluated by radio-HPLC. It was found that [18F]fluoroethyl bufalin still had an excellent radio chemical purity after culture for 6 h (>95%; Figure 2B). The above results show the good in vitro stability of the compound in both injection solution and serum.

Biodistribution studies

The biodistribution of the [18F]fluoroethyl bufalin was conducted in nude mice bearing SMMC-7721 and HepG2 tumors; the findings are shown in Table 1 and Figure 3.

In SMMC-7721 hepatocellular carcinoma-bearing mice (Figure 3A), tumor uptake of 2.31%±0.71%ID/g was observed at 45 min pi and then it was increased slowly to 4.63%±0.94%ID/g at 2 h and decreased to 4.24%±0.86%ID/g at 4 h after injection. The results indicated that [18F]fluoroethyl bufalin in the liver was significantly higher than other organs, which reached 15.79%±0.73%ID/g at 45 min and then declined to 11.46%±3.3%ID/g at 2 h. Till 4 h, there was still an intense accumulation of 7.51%±1.17%ID/g. Activity accumulation in the kidneys decreased slowly from 7.17%±0.34%ID/g (45 min) to 3.21%±0.57%ID/g (2 h) after injection because of the excretion of the tracer into the urinary bladder. Blood CL fell rather promptly over time and presented low blood activity (1.82%±0.22%ID/g) at 2 h after injection.

In HepG2 hepatocellular carcinoma-bearing mice (Figure 3B), tumor uptake (2.59%±0.64%ID/g) was observed at 45 min pi and then increased slowly to 4.69%±0.92%ID/g and declined to 4.27%±0.50%ID/g at 2 and 4 h pi. These results indicated that [18F]fluoroethyl bufalin uptake in liver was significantly higher than other organs, which reached 19.74%±0.28%ID/g at 45 min and then declined to 10.46%±0.44%ID/g at 2 h. At 4 h, there was still an intensity accumulation of 7.51%±1.17%ID/g.

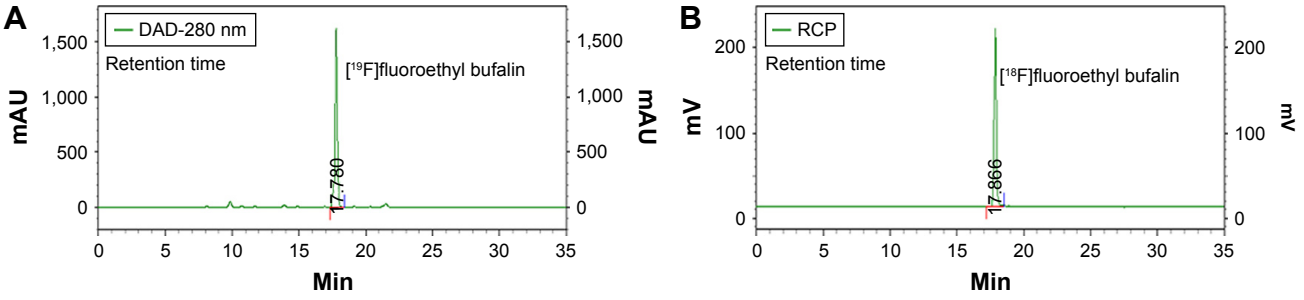

Figure 1 HPLC chromatogram of [19F]fluoroethyl bufalin and [18F]fluoroethyl bufalin.
Notes: HPLC chromatogram of (isocratic, 0.05 mol/L phosphate buffer [pH =7.0], flow 1 mL/min) (**A**) [19F]fluoroethyl bufalin, T_R =17.78 min (UV =280 nm) and (**B**) [18F]fluoroethyl bufalin, T_R =17.86 min.
Abbreviations: DAD, diode array detector; HPLC, high-performance liquid chromatography; RCP, radiochemical purity; T_R, retention time; UV, ultraviolet.

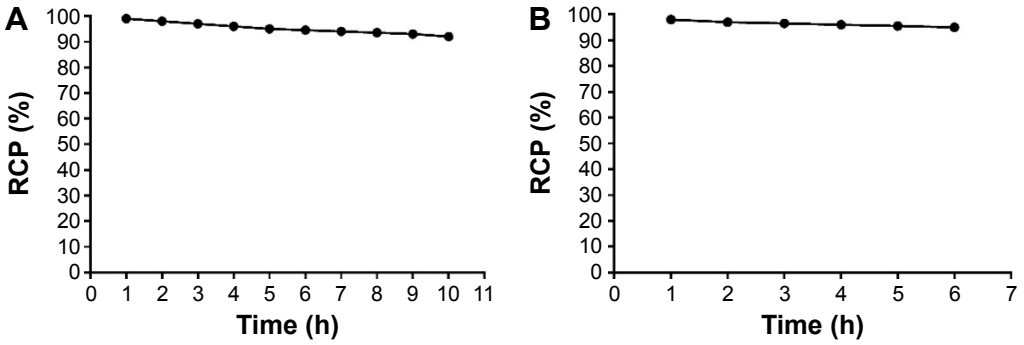

Figure 2 Stability of [^{18}F]fluoroethyl bufalin at different intervals in 0.1 mol/L PBS (**A**) and mouse serum (**B**).
Abbreviations: PBS, phosphate-buffered saline; RCP, radiochemical purity.

Table 1 Biodistribution of [^{18}F]fluoroethyl bufalin in nude mice

Tissue	SMMC-7721			HepG2		
	45 min	120 min	240 min	45 min	120 min	240 min
Tumor	2.31±0.71	4.63±0.94	4.24±0.86	2.59±0.64	4.69±0.92	4.27±0.50
Blood	2.24±0.71	1.93±0.45	1.82±0.22	2.57±0.49	2.54±0.29	1.85±0.37
Heart	4.06±0.38	4.31±0.30	2.64±0.32	4.06±0.38	4.31±0.30	3.66±0.72
Liver	15.79±0.73	11.46±1.3	7.51±1.17	19.74±0.28	10.46±0.44	6.51±1.17
Spleen	3.49±1.49	2.79±1.00	1.82±0.16	3.95±0.80	2.85±0.19	1.69±0.13
Lung	3.66±0.72	3.10±0.20	2.57±0.38	3.43±1.17	3.04±0.29	2.91±0.22
Kidney	7.17±0.34	4.21±0.29	3.21±0.57	7.88±0.42	4.32±0.43	3.67±0.51
Stomach	3.51±0.93	2.73±0.36	1.46±0.13	3.43±0.79	2.57±0.38	1.51±0.07
Intestine	4.45±0.34	4.50±0.55	4.73±0.88	3.10±0.54	4.92±0.65	5.24±0.19
Femur	3.19±2.07	3.65±0.13	6.55±2.21	2.21±0.5	3.87±0.37	6.61±1.30
Muscle	2.76±0.48	3.63±0.94	3.24±0.86	2.08±0.42	3.01±0.23	2.40±0.54
Brain	4.27±0.50	4.13±0.42	3.96±0.11	3.44±0.44	4.04±0.45	3.54±0.37
Tumor/liver	0.15±0.97	0.40±0.72	0.56±0.74	0.13±2.28	0.45±2.09	0.66±0.43

Notes: Radioactivity accumulation was expressed as %ID/g after a single intravenous injection of 7.4 MBq of [^{18}F]fluoroethyl bufalin in 0.5 mL at 45, 120, and 240 min (n=5/group, mean ± SD). %ID/g, percentage of injected dose per gram of tissue per body weight.

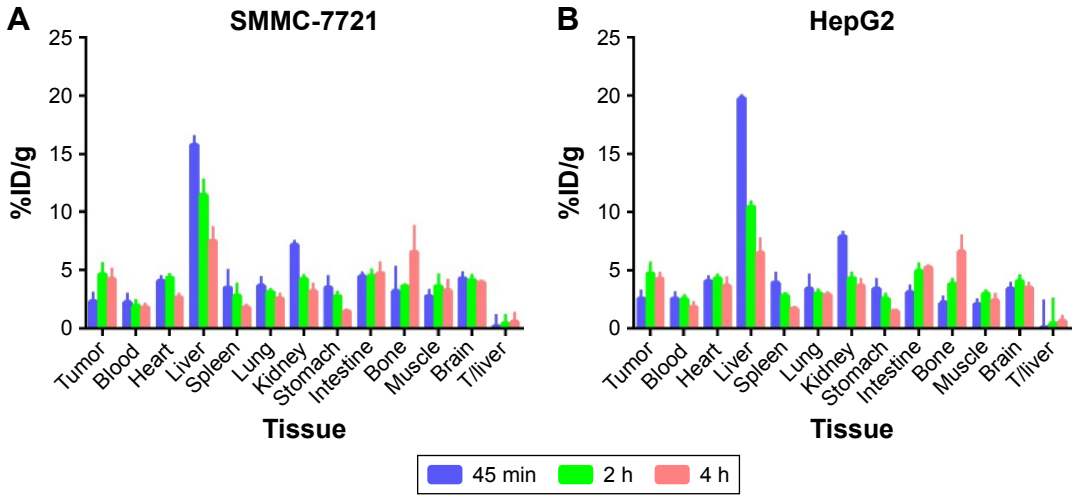

Figure 3 Biodistributions of [^{18}F]fluoroethyl bufalin in SMMC-7721 (**A**) and HepG2 (**B**) xenograft-bearing nude mice.
Notes: SMMC-7721 (**A**) and HepG2 (**B**) mice were injected with 7.4 MBq of [^{18}F]fluoroethyl bufalin, and biodistribution was studied at 45, 120 and 240 min after injection. Radioactivity accumulation was expressed as %ID/g after a single intravenous injection of 7.4 MBq of [^{18}F]fluoroethyl bufalin in 0.5 mL at 45, 120, and 240 min (n=5/group, mean ± SD). %ID/g, percentage of injected dose per gram of tissue per body weight.
Abbreviation: T, tumor.

Activity accumulation in the kidneys decreased slowly from 45 min (7.17%±0.34%ID/g) to 2 h (3.21%±0.57%ID/g) after injection because of the excretion of the tracer into the urinary bladder. Blood CL fell rather promptly over time and presented low blood activity (1.85%±0.37%ID/g) in 2 h after injection.

The tracer uptake accumulated in the SMMC-7721 tumors, HepG2 tumors, and the major tissues. The uptake of [18F]fluoroethyl bufalin in the liver was considerably higher than that in other tissues, for instance, the lung, stomach, spleen, and intestine at three time points. Rapid body CL from the circulation was mostly by the hepatic and renal pathways.

Pharmacokinetic studies

Table 2 shows the pharmacokinetic parameters, attained by the pharmacokinetic calculation program. Figure 4 shows the concentration–time curves of [18F]fluoroethyl bufalin in the ICR mice till 10 h after injection. The pharmacokinetic profiles of [18F]fluoroethyl bufalin fitted a two-compartment open model the best. The pharmacokinetic equation was as follows:

$$C = 39.983e^{-1t} + 1.247e^{-0.001t}$$

where C is radiopharmacokinetic activity (%ID/g) in plasma and t is the time after injection.

The values of AUC_{0-t} and CL were 540.137 μg/L·min and 0.001 L/min/kg, respectively. The half-life of distribution ($t_{1/2\alpha}$) and half-life of elimination ($t_{1/2\beta}$) were 0.693 and 510.223 min, respectively. The results revealed that [18F]fluoroethyl bufalin could be absorbed rapidly and eliminated slowly.

Table 2 Pharmacokinetic parameters of the [18F]fluoroethyl bufalin in ICR mice

Parameter (units)	[18F]fluoroethyl bufalin
K_{10} (min^{-1})	0.048
K_{12} (min^{-1})	0.921
K_{21} (min^{-1})	0.038
Vd (Vd)	0.029
CL (L/min/kg)	0.001
$t_{1/2\alpha}$ (min)	0.693
$t_{1/2\beta}$ (min)	510.223
$AUC_{(0-t)}$ (μg/L·min)	540.137
$AUC_{(0-\infty)}$ (μg/L·min)	851.462

Notes: Pharmacokinetic parameters of [18F]fluoroethyl bufalin in the ICR mice till 10 h post injection. K_{10}, elimination rate constant; K_{12}, elimination rate constant from central compartment to peripheral compartment; K_{21}, elimination rate constant from peripheral compartment to central compartment; Vd, apparent volume of distribution.

Abbreviations: CL, clearance; AUC, area under concentration time–curve; ICR, Institute of Cancer Research; $t_{1/2\alpha}$, half-life of distribution; $t_{1/2\beta}$, half-life of elimination.

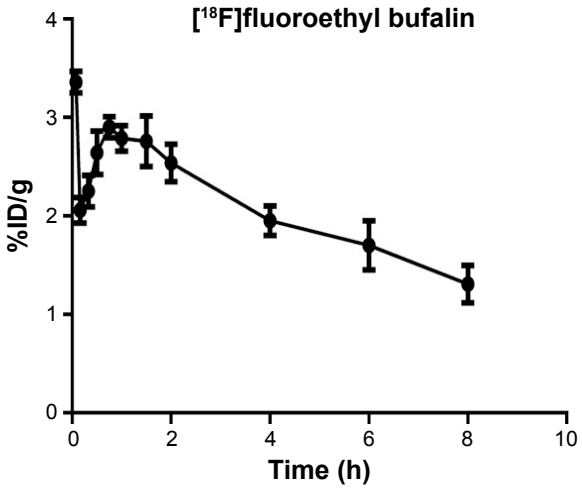

Figure 4 The blood drug concentration–time curve for [18F]fluoroethyl bufalin in the ICR mice.

Notes: The blood drug concentration–time curve for [18F]fluoroethyl bufalin in the ICR mice till 10 hour pi. %ID/g, percentage of injected dose per gram of tissue per body weight.

Abbreviations: ICR, Institute of Cancer Research; pi, post injection.

Micro-PET images in SMMC-7721 and HepG2 tumor-bearing nude mice

Figure 5 demonstrates characteristic PET images of the nude mice at different points of time pi of [18F]fluoroethyl bufalin. The PET study provided extra data relating to the distribution of not only the blood CL but also the precise tissue uptake of [18F]fluoroethyl bufalin in the course of scan during 240 min. In addition, the micro-PET imaging findings coincided with the results of the distribution studies.

Radioactivity uptake of SMMC-7721 tumor was detected started at 5 min pi. As shown in Figure 6A, SMMC-7721 tumor uptake remained steady over time (2.96±0.75, 4.38±0.37, 4.70±0.29, 3.63±0.94, 3.24±0.86, and 2.48%±0.57%ID/g at 5 min, 35 min, 55 min, 2 h, 4 h, and 6 h pi, respectively). The liver uptake reached a peak (30.15%±3.05%ID/g) at 5 min pi and then declined to 15.83%±2.75%ID/g at 60 min pi. Tracer uptake in the heart, lung, and other organs also correlated well with the distribution results. An appreciable radioactivity accumulation in the bladder (33.14%±5.81%ID/g) was noticed at 120 min pi.

Radioactivity uptake of HepG2 tumor was also detected starting at 5 min pi. As shown in Figure 6B, HepG2 tumor uptake remained steady over time (2.59±0.64, 3.19±0.37, 4.44±0.69, 4.18±0.99, and 2.75%±0.62%ID/g at 5 min, 35 min, 55 min, 2 h, 4 h, and 6 h pi, respectively), corroborating

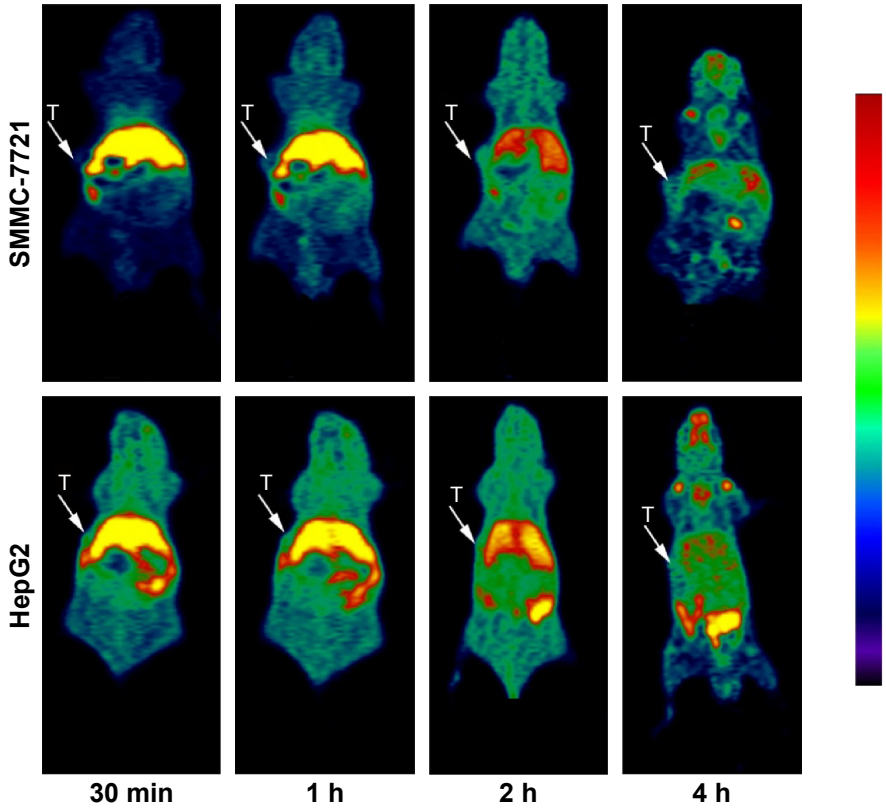

Figure 5 Dynamic small-animal PET scans obtained for [^{18}F]fluoroethyl bufalin with SMMC-7721 T-bearing mice and HepG2 T-bearing mice.
Notes: Coronal whole-body slices that contained Ts are shown; arrows indicate Ts.
Abbreviations: PET, positron emission tomography; Ts, tumors.

the distribution results. The liver uptake reached a peak (39.84%±2.77%ID/g) at 5 min pi and then declined to 5.42%±1.27%ID/g at 60 min pi. Tracer uptake in the heart, lung, and other organs also correlated well with the distribution results. An appreciable radioactivity accumulation in the bladder (15.75%±1.9%ID/g) was noticed at 120 min pi. In the course of the initial part of this research, noticeable liver uptake was calculated, which suggests that hepatic metabolism was through the main excretory system. Elimination was also through the renal system, because of the marked CL to

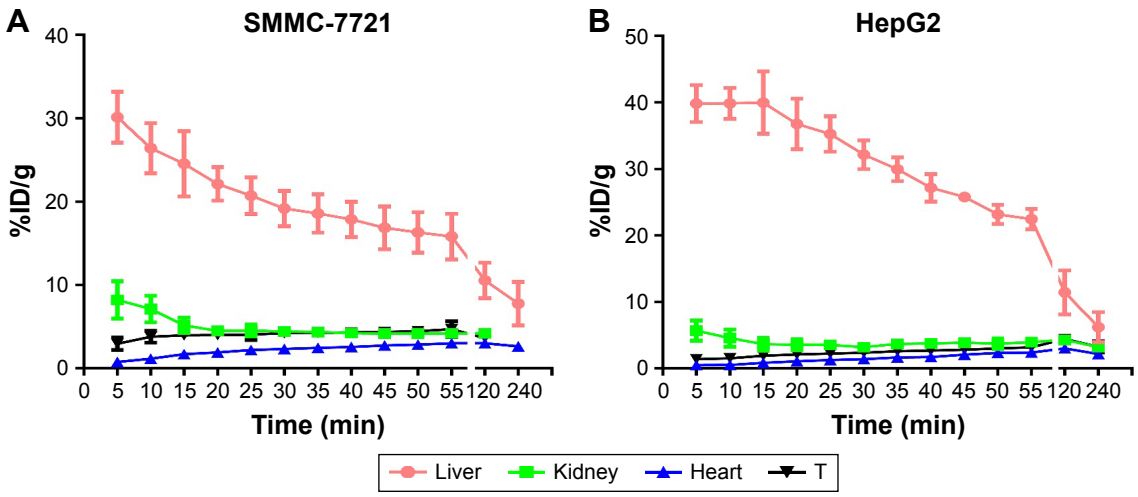

Figure 6 Quantified time–activity curves of major organs in SMMC-7721 and HepG2 T-bearing mice.
Notes: (**A**) Quantified time–activity curves of major organs (T, liver, heart, and kidney) after injection of 7.4 MBq [^{18}F]fluoroethyl bufalin in SMMC-7721 T-bearing mice (n=3). (**B**) Quantified time–activity curves of major organs (T, liver, heart, and kidney) after injection of 7.4 MBq [^{18}F]fluoroethyl bufalin in HepG2 T-bearing mice (n=3). %ID/g, percentage of injected dose per gram of tissue per body weight.
Abbreviation: T, tumor.

the bladder and short kidney maintenance, indicating that [18F]fluoroethyl bufalin was rapidly excreted through both renal and hepatobiliary routes. In two tumor models, PET images demonstrated similar distributions in all organs.

Discussion

In this study, [18F]fluoroethyl bufalin was prepared successfully and proved to be stable in mouse serum. These properties warranted its in vivo PET imaging. From the tissue biodistribution studies, it was found that high uptake of [18F]fluoroethyl bufalin was detected in the liver which would be due to high lipophilic property and other possible mechanisms of bufalin in vivo.

To better interpret PET imaging results, first we have to understand bufalin and its possible tumor treatment mechanism. It is known that cytochrome P450 3A4 (CYP3A4), a member of the cytochrome P450 mixed-function oxidase system, is one of the most significant enzymes involved in the metabolism of drugs in the body. CYP3A4 accounts for ~40% of the total cytochrome P450 in human liver microsomes and metabolizes >50% of the clinically used drugs.[19] Earlier research has also shown that bufalin had a modest but significant inhibition of CYP3A4 enzyme both in vitro and in vivo.[20] As a result, the high CYP3A4 enzyme metabolic capability in liver would be a probable explanation for the extremely high concentration of bufalin and [18F]fluoroethyl bufalin in liver. Additional risk would arise when the drug involved has a narrow therapeutic index, and further experiments are required to be carried out to determine whether bufalin could be metabolized by the liver system or whether its metabolites could inhibit the CYP3A4 enzyme.

Previous study demonstrated that bufalin inhibited the proliferation of SMMC-7721 and HepG2 human hepatocellular carcinoma cell lines in a dose-dependent and time-dependent manner and therefore would induce G2/M phase cell cycle arrest,[21] induce the proteins for the mitochondria-mediated apoptosis,[22] and inhibit the AKT/GSK3 beta/beta-catenin/E-cadherin signaling pathway.[11]

Moreover, bufalin reduced the proliferation of HepG2 and SMMC-7721 hepatocellular carcinoma cells, which was relevant to the expression of Na^+/K^+-ATPase $\alpha 3$,[23] because the protein expression of Na^+/K^+-ATPase $\alpha 3$ was at the same level in SMMC-7721 and HepG2 cells.[23,24] This information can also support that tumor uptake of [18F]fluoroethyl bufalin in SMMC-7721 and HepG2 tumor-bearing mice was similar in tissue distribution and PET imaging studies. The expression of Na^+/K^+-ATPase may be the reason of the drug uptake in tumor, and the mechanism needs to be further studied.

Interestingly, as observed in Figure 3, differences were observed in concentration–time curves of [18F]fluoroethyl bufalin. The AUC_{0-t} of double peaks suggested that enterohepatic recirculation might have occurred.[25] The double-peak phenomenon reported here was in agreement with previous reports.[26] Previous pharmacokinetic research presented an analogous phenomenon in rats.[27] It is known that drug absorption is a complicated course. The pharmacokinetic results manifest that [18F]fluoroethyl bufalin may be through potential interaction. More detailed pharmacokinetic research is needed to reveal the mechanism of the double-peak phenomenon.

These results of the imaging examination disclosed that [18F]fluoroethyl bufalin momentarily accumulated in the liver pi; most of the [18F]fluoroethyl bufalin actually accumulated in the liver at 5 min and then decreased slowly with time moving forward. At 120 min, there was still more than one-third of [18F]fluoroethyl bufalin in the liver compared to the level at 5 min. Therefore, these findings demonstrated that [18F]fluoroethyl bufalin was trapped in the liver. Some studies suggested that the intestine, liver, and kidney might be the major distributive organs of bufalin in vivo after oral administration.[25] In this study, however, we found that the liver was actually the major accumulated site for this drug, while kidneys transmitted this drug to the urinary bladder quickly, which could account for high accumulation of the drug in mice bladders. A previous study had shown that bufalin prevented the migration and invasion of T24 bladder carcinoma cells through the inactivation of matrix metalloproteinases.[28] Combined with our study, it is suggested that bufalin may be a promising therapeutic agent for bladder disease.

Conclusion

In the present research, we coupled bufalin with 18F through the labeling intermediate $^{18}F\text{-}CH_2CH_2OTs$. The pharmacokinetic parameters of [18F]fluoroethyl bufalin were achieved and showed fast CL in vivo. The real-time imaging data showed that [18F]fluoroethyl bufalin temporarily accumulated in the liver and was excreted mainly through both hepatic pathway and renal pathway. There was moderate uptake of [18F]fluoroethyl bufalin in two HCC tumors. Long-term accumulation of the tracer was not found in the organs. These results not only were helpful for the understanding of in vivo behavior of bufalin in clinical practices but also provided scientific information for monitoring bufalin therapy efficacy.

Acknowledgments

This work was jointly supported by the Traditional Chinese Medicine Research Fund of Shanghai Municipal Commission

of Health and Family Planning (Number: 2014JP009A), the Three Years Program of Shanghai Municipal Traditional Chinese Medicine (Number: ZY3-CCCX-3-30036), and the Carcinogenesis and Cancer Invasion Laboratory of Education Ministry of China. This work was also supported in part by grants from the National Natural Science Foundation of China (81471706 and 81201130) and Shanghai Municipal Commission of Health and Family Planning (XYQ2013106). We sincerely thank Doctor Dong-Mei Gao and Jun Chen (Liver Cancer Institute, Zhongshan Hospital, Fudan University, Shanghai, People's Republic of China) for their expert support in cell culture and animal model. We also thank Doctor Weizhong Wu (Liver Cancer Institute, Zhongshan Hospital, Fudan University, Shanghai, People's Republic of China) for his assistance with the animal model experiments.

Disclosure

The authors report no conflicts of interest in this work.

References

1. Krenn L, Kopp B. Bufadienolides from animal and plant sources. *Phytochemistry*. 1998;48(1):1–29.
2. Hu F, Han J, Zhai B, et al. Blocking autophagy enhances the apoptosis effect of bufalin on human hepatocellular carcinoma cells through endoplasmic reticulum stress and JNK activation. *Apoptosis*. 2014;19(1):210–223.
3. Qiu Y, Hu Q, Tang Q, et al. MicroRNA-497 and bufalin act synergistically to inhibit colorectal cancer metastasis. *Tumor Biol*. 2014;35(3):2599–2606.
4. Jing Y, Watabe M, Hashimoto S, Nakajo S, Nakaya K. Cell cycle arrest and protein kinase modulating effect of bufalin on human leukemia ML1 cells. *Anticancer Res*. 1994;14(3A):1193–1198.
5. Li A, Qu X, Li Z, et al. Secreted protein acidic and rich in cysteine antagonizes bufalin induced apoptosis in gastric cancer cells. *Mol Med Rep*. 2015;12(2):2926–2932.
6. Chang Y, Zhao Y, Zhan H, Wei X, Liu T, Zheng B. Bufalin inhibits the differentiation and proliferation of human osteosarcoma cell line hMG63-derived cancer stem cells. *Tumor Biol*. 2014;35(2):1075–1082.
7. Shen S, Zhang Y, Wang Z, Zhang R, Gong X. Bufalin induces the interplay between apoptosis and autophagy in glioma cells through endoplasmic reticulum stress. *Int J Biol Sci*. 2014;10(2):212–224.
8. Tsai SC, Yang JS, Peng SF, et al. Bufalin increases sensitivity to AKT/mTOR-induced autophagic cell death in SK-HEP-1 human hepatocellular carcinoma cells. *Int J Oncol*. 2012;41(4):1431–1442.
9. Chen Y, Lu H, Hsu S, et al. Bufalin inhibits migration and invasion in human hepatocellular carcinoma SK-Hep1 cells through the inhibitions of NF-kB and matrix metalloproteinase-2/-9-signaling pathways. *Environ Toxicol*. 2015;30(1):74–82.
10. Zhang Z, Yang Y, Wu W. Bufalin attenuates the stage and metastatic potential of hepatocellular carcinoma in nude mice. *J Transl Med*. 2014;12(1):57.
11. Qiu D, Zhang Z, Wu W, Yang Y. Bufalin, a component in Chansu, inhibits proliferation and invasion of hepatocellular carcinoma cells. *BMC Complement Altern Med*. 2013;13(1):185.
12. Griffiths GL. The imaging probe development center and the production of molecular imaging probes. *Curr Chem Genomics*. 2008;1:65–69.
13. West CML, Jones T, Price P. The potential of positron-emission tomography to study anticancer-drug resistance. *Nat Rev Cancer*. 2004;4(6):457–469.
14. Gangloff A, Hsueh WA, Kesner AL, et al. Estimation of paclitaxel biodistribution and uptake in human-derived xenografts in vivo with (18)F-fluoropaclitaxel. *J Nucl Med*. 2005;46(11):1866–1871.
15. Zhang M, Kumata K, Hatori A, et al. [11C]Gefitinib ([11C]Iressa): radiosynthesis, in vitro uptake, and in vivo imaging of intact murine fibrosarcoma. *Mol Imaging Biol*. 2010;12(2):181–191.
16. Nagengast WB, de Korte MA, Oude Munnink TH, et al. 89Zr-Bevacizumab PET of early antiangiogenic tumor response to treatment with HSP90 inhibitor NVP-AUY922. *J Nucl Med*. 2010;51(5):761–767.
17. Woodcock J, Woosley R. The FDA critical path initiative and its influence on new drug development. *Annu Rev Med*. 2008;59(1):1–12.
18. Marchetti S, Schellens JHM. The impact of FDA and EMEA guidelines on drug development in relation to Phase 0 trials. *Br J Cancer*. 2007;97(5):577–581.
19. Luo G, Cunningham M, Kim S, et al. CYP3A4 induction by drugs: correlation between a pregnane X receptor reporter gene assay and CYP3A4 expression in human hepatocytes. *Drug Metab Dispos*. 2002;30(7):795–804.
20. Li H, Xu W, Zhang X, Zhang W, Hu L. Bufalin inhibits CYP3A4 activity in vitro and in vivo. *Acta Pharmacol Sin*. 2009;30(5):646–652.
21. Xie RF, Li ZC, Gao B, Shi ZN, Zhou X. Bufothionine, a possible effective component in cinobufocini injection for hepatocellular carcinoma. *J Ethnopharmacol*. 2012;141(2):692–700.
22. Xie R, Li Z, Chen P, Zhou X. Bufothionine induced the mitochondria-mediated apoptosis in H-22 liver tumor and acute liver injury. *Chin Med*. 2015;10:5.
23. Li H, Wang P, Gao Y, et al. Na+/K+-ATPase alpha3 mediates sensitivity of hepatocellular carcinoma cells to bufalin. *Oncol Rep*. 2011;25(3):825–830.
24. Blanco G. Na,K-ATPase subunit heterogeneity as a mechanism for tissue-specific ion regulation. *Semin Nephrol*. 2005;25(5):292–303.
25. Roberts MS, Magnusson BM, Burczynski FJ, Weiss M. Enterohepatic circulation. *Clin Pharmacokinet*. 2002;41(10):751–790.
26. Huang H, Yang Y, Lv C, et al. Pharmacokinetics and tissue distribution of five bufadienolides from the Shexiang Baoxin pill following oral administration to mice. *J Ethnopharmacol*. 2015;161:175–185.
27. Liang Y, Liu A, Qin S, et al. Simultaneous determination and pharmacokinetics of five bufadienolides in rat plasma after oral administration of Chansu extract by SPE-HPLC method. *J Pharm Biomed*. 2008;46(3):442–448.
28. Hong SH, Kim GY, Chang YC, Moon SK, Kim WJ, Choi YH. Bufalin prevents the migration and invasion of T24 bladder carcinoma cells through the inactivation of matrix metalloproteinases and modulation of tight junctions. *Int J Oncol*. 2013;42(1):277–286.